

Transport through correlated quantum dots: An investigation using the functional renormalization group

Michael Weyrauch and Dieter Sibold

*Physikalisch-Technische Bundesanstalt, D-38116 Braunschweig, Germany**

(Dated: December 1, 2018)

Calculations using the (exact) fermionic functional renormalization group are usually truncated at the second order of the corresponding hierarchy of coupled ordinary differential equations. We present a method for the systematic determination of higher order vertex functions. This method is applied to a study of transport properties of various correlated quantum dot systems. It is shown that for large Coulomb correlations higher order vertex functions cannot be neglected, and a static approximation is insufficient.

PACS numbers: 73.63.Kv, 73.23.Hk

I. INTRODUCTION

Recently, electron transport through ultrasmall fermionic systems (quantum dots) has been investigated intensively^{1,2,3,4,5}. Motivation for these studies is the potential application of quantum dots to quantum computers and quantum measurement devices⁶. The transport process can be described using the concept of Coulomb blockade, when Coulomb correlations are large compared to other energy scales in the quantum dot system. However, a detailed analysis of the conductance and level occupancies of the quantum dot states as a function of an applied gate voltage shows a rich structure, which is related to Kondo physics. The theoretical description of such effects requires non-perturbative methods, and many studies employ Wilson's numerical renormalization group (NRG). Recently, functional renormalization group techniques have emerged as a new non-perturbative tool to describe mesoscopic phenomena theoretically^{3,4}.

While the functional renormalization group equation (fRG) is exact in principle, for practical applications it must be truncated⁷. In particular, most fRG investigations of mesoscopic systems use a static approximation (i.e. energy independent self-energies and higher vertex functions), and the hierarchy of differential equations corresponding to the fRG is truncated at second order. Since fRG calculations truncated at second order are quite 'cheap' numerically in comparison to NRG or DMRG (density matrix renormalization group) calculations, it is possible to map out the potentially huge parameter space of quantum dot systems with reasonable effort. Functional renormalization group calculations beyond the static approximation are technically difficult and require a significant numerical effort as is demonstrated in model studies for single quantum particles^{8,9}.

The uncertainties incurred by the truncation of the fRG are not easily controlled. Therefore, it is worth studying the static approximation beyond second order truncation. Moreover, methods to go beyond the static approximation with reasonable effort should be developed, and the limits of the static approximation should

be assessed.

It is the purpose of the present paper to investigate the influence of vertex functions beyond second order in a static approximation. To this end, we develop a method which enables to extract the complete set of ordinary differential equations from the underlying functional differential equation (section II). Our method uses a different regularization scheme than the one usually employed for fermionic systems, which regularizes the free propagator (see e.g. Refs. 8 and 10). Our cutoff procedure is adapted from the scheme used in Ref. 7, which adds a regulator to the action. We are able to show that the two procedures yield the same set of ordinary coupled differential equations for the standard hard cutoff regulator. Furthermore, it is shown that this set is finite in principle for a fermionic system. (This is in contrast to Bose systems where this set is infinite.) The number of differential equations obtained nevertheless grows exponentially with the number of degrees of freedom of the mesoscopic system under consideration.

For quantum dot systems described by only a small number of electronic states, a study considering all possible vertex functions is feasible (within the constraints of the static approximation). In this way, the limits of the static approximation can be assessed. In order to do that we investigate transport properties of various quantum dot devices with different couplings to the external leads (section III). It is shown that consideration of higher order vertex functions is important in order to describe transport properties of correlated quantum dots quantitatively, in particular for systems with strong Coulomb correlations. However, in many cases we find that the set of differential equations to be solved develops singularities if we increase Coulomb correlations beyond some critical value, and the renormalization flow becomes unphysical. This is, of course, not unexpected, and just shows that for a quantitative analysis of mesoscopic systems with strong Coulomb correlations one eventually needs to go beyond the static approximation. This will be addressed in a forthcoming publication using the methods developed here but including a wave function renormalization in the kinetic energy term of the action.

II. FUNCTIONAL RG SCHEME FOR INTERACTING FERMIONS

The effective average action Γ_k for interacting Fermions evolves according to the functional renormalization group equation^{7,11}

$$\frac{\partial}{\partial k} \Gamma_k[\phi^*, \phi] = -\frac{1}{2} \text{Tr} \left\{ [\Gamma_k^{(2)}[\phi^*, \phi] + R_k]^{-1} \frac{\partial R_k}{\partial k} \right\}. \quad (1)$$

Here, we assume that the space of possible states of the Fermions is suitably discretized, so that a N -component vector of Grassmann variables $\phi(\tau) = (\phi_1(\tau), \dots, \phi_N(\tau))$ describes the evolution of the interacting Fermion system in imaginary time τ . Each index $\alpha \in \{1, \dots, N\}$ represents all quantum numbers necessary to completely specify a Fermionic state, e.g. spin projection σ and position j in a linear chain of electrons. The functional derivative of Γ_k with respect to ϕ^* and ϕ is denoted by $\Gamma_k^{(2)}$. The regulator R_k is introduced in order to suppress thermal and quantum fluctuations at energy or momentum scales k larger than any physical scale relevant for the problem that is being investigated. With decreasing k , the regulator gradually “switches on” such fluctuations until they are fully included at $k = 0$, i.e. at $k = 0$ the regulator R_k vanishes. A concrete choice for R_k will be discussed below. The initial condition for the evolution described by Eq. (1) is obtained from the Hamiltonian defining the problem to be solved⁷. The trace in Eq. (1) is to be performed over all relevant quantum numbers.

In order to solve a functional differential equation like Eq. (1) in practice, it must be truncated. This essentially entails a suitable transformation of the functional differential equation into an infinite set of coupled partial or ordinary differential equations. This set of differential equations is then truncated at a suitable order. The standard technique expands both sides of the equation for the effective average into a Taylor series about a τ independent vector ϕ_0 using $\phi(\tau) = \phi_0 + \psi(\tau)$. One then obtains an infinite set of ordinary or partial differential equations for the Taylor coefficients of the various powers in $\psi(\tau)$.

For most practical applications, the truncation procedure described so far is still too general, and we need further simplifications: One standard way to proceed is to prescribe the functional form of the effective average action more specifically: In this paper we assume that the effective average action takes the form

$$\Gamma_k[\phi^*, \phi] = \int_0^\beta d\tau \sum_{\alpha=1}^N \phi_\alpha^*(\tau) \frac{\partial}{\partial \tau} \phi_\alpha(\tau) + U_k(\phi^*(\tau), \phi(\tau)) \quad (2)$$

where the ‘effective potential’ U_k does not depend on derivatives of the Grassmann variables with respect to the imaginary time τ . Assuming the specific form (2) yields energy independent (static) self-energies and higher order vertex functions. Of course, more general functional forms for Γ_k lead to energy dependent vertex functions [e.g. a wave function renormalization

$Z_k(\phi^*(\tau), \phi(\tau))$ multiplying the kinetic energy term in Eq. (2)], but such a truncation will not be investigated in this paper.

Since the effective potential U_k must be a Grassmann scalar, its form in terms of $\phi(\tau)$ is fairly well determined: It must be a linear combination of all possible products of elements of the set of Grassmann variables $\{\phi_\alpha^*, \phi_\alpha\}$ with an even number of factors. Due to the nil-potency of the Grassmann variables the number of possible products is finite, i.e. the number of terms in the linear combinations is finite. Since the number of particles is conserved in the physical models that we want to investigate, we only need to include terms with an equal number of ϕ_α^* and ϕ_α , which correspond to Fermion creation and destruction, respectively.

Here is an example for $N = 2$: Due to the nil-potency of the Grassmann variables, the effective potential has the general form

$$U_k(\phi^*, \phi) = a_{0,k} + \phi_1^* \phi_{11,k} + \phi_2^* \phi_{22,k} + \phi_1^* \phi_2 a_{12,k} + \phi_2^* \phi_1 a_{21,k} + \phi_1^* \phi_2^* \phi_1 \phi_2 a_{1212,k}. \quad (3)$$

The k -dependent coefficients in this expression will be called ‘running couplings’. The running couplings have direct physical significance: Since the effective average action at $k = 0$ is the generator of the vertex functions, each running coupling corresponds to an n -point vertex function, where n corresponds to its number of Grassmann factors. In particular, a_0 is directly related to the ground state energy of the Fermion system, and the $a_{ij,k}$ correspond to the self-energies. For simplicity, the k -dependence of the couplings will not always be explicitly indicated.

Following the general procedure outlined above, we will now determine flow equations for the running couplings. To this end we first expand the effective average action (2) about τ -independent Grassmann variables $\phi_0 = (\phi_{01}, \dots, \phi_{0N})$, i.e. $\phi_\alpha(\tau) = \phi_{0\alpha} + \psi_\alpha(\tau)$ with $\phi_{0\alpha} = \phi_\alpha(0)$. Up to second order in $\psi_\alpha(\tau)$, the expansion is given by

$$\begin{aligned} \Gamma_k[\phi^*, \phi] &= \beta U_k^{(0)}(\phi_0^*, \phi_0) \\ &+ \frac{1}{2} \int_0^\beta d\tau \int_0^\beta d\tau' \Psi^\dagger(\tau) \gamma_k^{(2)}(\phi_0^*, \phi_0) \Psi(\tau') \\ &+ \dots \end{aligned} \quad (4)$$

with $\Psi(\tau) = (\psi_1(\tau), \dots, \psi_N(\tau), \psi_1^*(\tau), \dots, \psi_N^*(\tau))$. The lowest order term is determined by the effective potential

$$U_k^{(0)}(\phi_0^*, \phi_0) = U_k(\phi^*(\tau), \phi(\tau))|_{\psi^*=\psi=0}. \quad (5)$$

The second order term contains the second derivative of the effective potential

$$\begin{aligned} \gamma_k^{(2)}(\phi_0^*, \phi_0) &= \left(\mathbb{E}' \partial_\tau + U_k^{(2)}(\phi_0^*, \phi_0) \right) \delta(\tau - \tau'), \\ U_{k,\alpha\beta}^{(2)}(\phi_0^*, \phi_0) &= \left. \frac{\partial^2 U_k}{\partial \Psi_\alpha \partial \Psi_\beta^\dagger} \right|_{\psi^*=\psi=0} \end{aligned} \quad (6)$$

with $\mathbb{E}' = \text{diag}(1, \dots, 1, -1, \dots, -1)$. The term in first order in Ψ drops out. For example, for $N = 2$ assuming

$$U_k^{(2)} = \begin{pmatrix} a_{11} - \phi_{02}^* \phi_{02} a_{1212} & a_{12} + \phi_{02}^* \phi_{01} a_{1212} & 0 & \phi_{01} \phi_{02} a_{1212} \\ a_{12} + \phi_{01}^* \phi_{02} a_{1212} & a_{22} - \phi_{01}^* \phi_{01} a_{1212} & -\phi_{01} \phi_{02} a_{1212} & 0 \\ 0 & \phi_{01}^* \phi_{02}^* a_{1212} & -a_{11} + \phi_{02}^* \phi_{02} a_{1212} & -a_{12} - \phi_{01}^* \phi_{02} a_{1212} \\ -\phi_{01}^* \phi_{02}^* a_{1212} & 0 & -a_{12} - \phi_{02}^* \phi_{01} a_{1212} & -a_{22} + \phi_{01}^* \phi_{01} a_{1212} \end{pmatrix} \quad (7)$$

In order to do the τ -integration in Eq. (4) we Fourier transform the Grassmann variables ψ_α using

$$\psi_\alpha(\tau) = \frac{1}{\sqrt{\beta}} \sum_n e^{i\omega_n \tau} \psi_{\alpha,n} \quad (8)$$

with the fermionic Matsubara frequency $\omega_n = (2n + 1)\pi/\beta$ and obtain for the effective average action

$$\Gamma_k[\phi^*, \phi] = \beta U_k^{(0)} + \frac{1}{2} \sum_{n=-\infty}^{\infty} \Psi_n^\dagger (i\omega_n \mathbb{E} + U_k^{(2)}) \Psi_n. \quad (9)$$

Here \mathbb{E} denotes the unit matrix. Moreover, we assume a regulator which is diagonal in Matsubara frequency space

$$\sum_n \psi_n^* R_{k,n} \psi_n = \frac{1}{2} \sum_n \Psi_n^\dagger R_{k,n} \mathbb{E}' \Psi_n. \quad (10)$$

Inserting Γ_k and R_k into Eq. (1) and comparing terms up to order zero in ψ we obtain the following equation

$$\frac{\partial}{\partial k} U_k^{(0)} = -\frac{1}{2\beta} \sum_n \text{Tr} K^{-1} \frac{\partial}{\partial k} R_{k,n}. \quad (11)$$

with $K = (i\omega_n + U_k^{(2)})\mathbb{E}' + R_{k,n}\mathbb{E}$. From this equation we extract a set of ordinary differential equations for the various coupling constants by comparing the coefficients of the various monomials of Grassmann variables. In order to do this, it is necessary to invert the Grassmann matrix K . The matrix is inverted using the formula

$$K^{-1} = (K_0 + K_1)^{-1} = K_0^{-1} \sum_{m=0}^N (-K_1 K_0^{-1})^m \quad (12)$$

where K_0 is chosen to be the body of K (Grassmann scalar part of K) and K_1 its soul (Grassmann non-scalar part). That the sum in Eq. (12) only runs up to N is due to the fact that each matrix element of K_1 is bilinear in the Grassmann variables, so that after N factors of K_1 the sum must terminate. Obviously, the inverse of K does not exist if the determinant of the body of K vanishes. In this case, the renormalization scheme is not well defined.

At $T = 0$ the sum over the Matsubara frequencies in Eq. (11) converts into an integral

$$\frac{1}{\beta} \sum_n \rightarrow \int_{-\infty}^{\infty} \frac{d\omega}{2\pi}. \quad (13)$$

the symmetry $a_{12} = a_{21}$, one easily finds from Eq. (3) the matrix

This integral is most easily evaluated for the sharp cut-off regulator

$$R_k(\omega) = Ck\theta(k^2 - \omega^2) \quad (14)$$

with C a suitably chosen large constant. This regulator fulfills the general requirements that it vanishes for $k = 0$ and it dominates the effective average action for $k \rightarrow \infty$. Furthermore, it has the advantage that the integration over the Matsubara frequencies can be done analytically. Some technical issues related to this integration will be discussed in Appendix A.

An often used approach to the fermionic functional renormalization group applies a hard cutoff in such a way that the free propagator at large k is suppressed, and propagation is gradually 'switched on' when k is reduced (see e.g. Refs. 10 and 8). In the following we shall see that this (standard) method and the cutoff employed here yield identical sets of flow equations.

With the results from Appendix A, we can write Eq. (11) for the hard cut-off regulator (14) in the following form

$$\frac{d}{dk} a_{0,k} = \frac{1}{4\pi} \sum_{\lambda=\pm k} \log \det \left(\frac{1}{k} G_k^{-1}(i\lambda) \right), \quad (15)$$

$$\frac{d}{dk} (U_k^{(0)} - a_{0,k}) = -\frac{1}{4\pi} \sum_{m=1}^N \sum_{\lambda=\pm k} \frac{1}{m} \text{Tr} (-M_k G_k(i\lambda))^m. \quad (16)$$

Eq. (16) represents a *finite* set of coupled ordinary differential equations for the running couplings. The block-diagonal $2N \times 2N$ matrix $G_k(i\lambda)$ is given by

$$G_k(i\lambda) = \begin{pmatrix} g_k(i\lambda) & 0 \\ 0 & g_k(-i\lambda) \end{pmatrix} = \begin{pmatrix} b_k(i\lambda) & 0 \\ 0 & b_k(-i\lambda) \end{pmatrix}^{-1}, \quad (17)$$

and the matrix elements of the $N \times N$ submatrix $b_k(i\lambda)$ are essentially determined by the self-energies

$$b_{\alpha\beta,k}(i\lambda) = a_{\alpha\beta,k} + i\lambda \delta_{\alpha\beta}. \quad (18)$$

The $2N \times 2N$ matrix M_k represents the soul of $U_k^{(2)}\mathbb{E}'$ and contains all running couplings except the self-energies.

Eqs. (15) and (16) are the main results of this section. From these results, the flow equations for the various

running couplings can be directly extracted up to the desired order by comparing the coefficients of the different monomials of Grassmann variables. As will be discussed further below, up to second order in m , Eqs. (15) and (16) are equivalent to results obtained in the literature using a hard cutoff on the free propagator. The advantage of Eqs. (15) and (16) is that they allow an easy and systematic construction of higher order contributions.

In order to illustrate the use of Eqs. (15) and (16), we extract the flow equations for $N = 2$ assuming the symmetry $a_{12} = a_{21}$ and purely real running couplings. In this case, the submatrix $g_k(i\lambda)$ is given by

$$g_k(i\lambda) = \frac{1}{b_{11}b_{22} - b_{12}^2} \begin{pmatrix} b_{22} & -b_{12} \\ -b_{12} & b_{11} \end{pmatrix} \quad (19)$$

with $b_{\alpha\beta}$ defined in Eq. (18). The matrix M_k can be directly read off from Eq. (7)

$$M_k = a_{1212,k} \begin{pmatrix} -\phi_{02}^* \phi_{02} & \phi_{02}^* \phi_{01} & 0 & \phi_{01} \phi_{02} \\ \phi_{01}^* \phi_{02} & -\phi_{01}^* \phi_{01} & -\phi_{01} \phi_{02} & 0 \\ 0 & -\phi_{01}^* \phi_{02}^* & -\phi_{02}^* \phi_{02} & \phi_{01}^* \phi_{02} \\ \phi_{01}^* \phi_{02}^* & 0 & \phi_{02}^* \phi_{01} & -\phi_{01}^* \phi_{01} \end{pmatrix}. \quad (20)$$

After some algebra one obtains the following flow equations for the various running couplings

$$\begin{aligned} a'_0 &= \frac{1}{\pi} \text{Re} \log (b_{11}b_{22} - b_{12}^2) / k^2, \\ a'_{ij} &= -\frac{a_{1212}}{\pi} \text{Re} \frac{b_{ij}}{b_{11}b_{22} - b_{12}^2}, \\ a'_{1212} &= -\frac{a_{1212}^2}{\pi} \text{Re} \frac{1}{b_{11}b_{22} - b_{12}^2} \\ &\quad - \frac{a_{1212}^2}{2\pi} \frac{b_{11}^* b_{22} + b_{11} b_{22}^* - 2b_{12} b_{12}^*}{(b_{11}b_{22} - b_{12}^2)(b_{11}^* b_{22}^* - b_{12}^{*2})}. \end{aligned} \quad (21)$$

The prime indicates a derivative with respect to k , and we do not indicate explicitly the k dependence of the running couplings.

For $N = 2$ the result Eq. (21) is complete within the static approximation. This means, that due to the finite number of Grassmann monomials which can be constructed from four Grassmann variables, there will be no higher order equations. The right hand side of the equations for a_{ij} arises from $m = 1$ in the sum over m in Eq. (16), while the right hand side of the equation for a_{1212} is the contribution from $m = 2$. Eqs. (21) are equivalent to Eqs. (26) and (27) in Ref. 4, where they are used to study electron transport through a single quantum dot. Moreover, the equations for a_{ij} in Eq. (21) are equivalent to Eq. (1) in Ref. 3 which was used to show that there are unusual correlation induced resonances in a polarized double dot system. (In order to show the equivalence one must set $a_{1212,k}$ to its initial condition $a_{1212,k} = U$.)

We now discuss the structure of the set of differential equations obtained from Eq. (16) for larger N using $N = 4$ as an example. As can be easily established, the

number of differential equations grows exponentially. In particular, for $N = 4$ we find 35 coupled equations corresponding to the number of Grassmann monomials we can build from 8 Grassmann variables in a system with particle conservation. If symmetries between these Grassmann monomials are considered the number of equations reduces, e.g. for a system of four electrons with spin symmetric interactions we only obtain 26 independent equations. It turns out that the resulting (complete) set of equations is quite formidable and can only be generated with the help of computer assisted symbolic computation. Nevertheless, some features of this set of equations can be established in general. These follow from the structure of Eq. (16): A term of order m in the sum over m in Eq. (16) only contributes to equations for coefficients with at least $2m$ indices. Such a term contains m propagators G_k . E.g., for $N = 4$, the term $m = 4$ in the sum over m only contributes to the equation for the running coupling $a_{12341234}$. Of course, the equation for this particular running coupling also receives contributions from $m = 1, 2, 3$.

To further illustrate the use of Eq. (16), we derive equations suitable for the description of a one dimensional chain of nearest neighbor coupled spinless electrons (see e.g., Ref. 12). To this end we first need to write down the effective potential in terms of the running couplings

$$\begin{aligned} U(\phi^*, \phi) &= \sum_{j=1}^N a_{jj} \phi_j^* \phi_j + a_{j,j+1} \phi_j^* \phi_{j+1} + a_{j,j-1} \phi_j^* \phi_{j-1} \\ &\quad + U \sum_{j=1}^N \phi_j^* \phi_j \phi_{j+1}^* \phi_{j+1} \end{aligned} \quad (22)$$

with periodic boundary conditions $\phi_0 = \phi_N$. Here, for simplicity, it is assumed that the density-density interaction strength U does not renormalize and remains at its initial value. In order to obtain the flow equations for the self-energies $a_{jj'}$, we consider the term $m = 1$ in the sum over m in Eq. (16). One easily finds

$$\begin{aligned} \text{Tr} M_k G_k &= U \sum_{j=1}^N [g_{j-1,j-1}(i\lambda) + g_{j+1,j+1}(i\lambda)] \phi_{0j}^* \phi_{0j} \\ &\quad - [g_{j,j+1}(i\lambda) \phi_{0j}^* \phi_{0j+1} + g_{j,j-1}(i\lambda) \phi_{0j}^* \phi_{0j-1}] \\ &\quad + (i\lambda \leftrightarrow -i\lambda). \end{aligned} \quad (23)$$

Inserting this result into Eq. (16) and comparing corresponding terms yields the flow equations

$$\begin{aligned} a'_{jj} &= \frac{U}{2\pi} \sum_{\lambda=\pm k} (g_{j+1,j+1}(i\lambda) + g_{j-1,j-1}(i\lambda)) \\ a'_{j,j\pm 1} &= -\frac{U}{2\pi} \sum_{\lambda=\pm k} g_{j,j\pm 1}(i\lambda) \end{aligned} \quad (24)$$

This result agrees with the one obtained using a hard cutoff on the free propagator; it is used to study e.g. persistent currents in mesoscopic rings in Ref. 12.

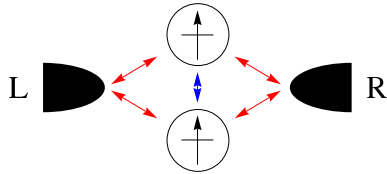


FIG. 1: (color online) Polarized double quantum dot coupled to left and right leads. The arrows between the dots and the leads symbolize the tunnel couplings t_j^l . The arrow between the dots symbolizes interdot Coulomb interactions.

III. TRANSPORT THROUGH CORRELATED QUANTUM DOTS

In the following we study transport through various quantum dot (QD) systems using the “effective potential” (i.e. static) approximation introduced in the previous section. We will emphasize the role of higher order contributions beyond $m = 2$ in the sum over m in Eq. (16). Up to $m = 2$, the equations resulting from Eq. (16) can be shown to be equivalent to the flow equations employed in Ref. 4. In order to elucidate the role of higher order contributions, we will study similar parameter sets as considered in Ref. 4. In some cases, calculations using Wilson’s numerical renormalization group are available for comparison.

The standard model Hamiltonian for the description of QD systems (depicted schematically in Fig. 1) consists of three essential terms: the dot Hamiltonian H_D , the Hamiltonian of the non-interacting electrons of the leads H_E and the interaction H_{DE} between the QD and the leads,

$$H = H_D + H_E + H_{DE}. \quad (25)$$

The dot Hamiltonian H_D is given by three terms

$$\begin{aligned} H_D = & \sum_{j\sigma} (\epsilon_{j\sigma} + V_g) d_{j\sigma}^\dagger d_{j\sigma} \\ & - \sum_{j>j',\sigma} t_{jj'} d_{j\sigma}^\dagger d_{j'\sigma} + h.c. \\ & + \frac{1}{2} \sum_{jj',\sigma\sigma'} U_{jj'}^{\sigma\sigma'} n_{j\sigma} n_{j'\sigma'} \end{aligned} \quad (26)$$

where $d_{j\sigma}^\dagger$ ($d_{j\sigma}$) creates (annihilates) an electron in state j with spin σ , respectively. The site occupancy operator is denoted by $n_{j\sigma} = d_{j\sigma}^\dagger d_{j\sigma}$. The dot levels $\epsilon_{j\sigma}$ may be shifted by application of a gate voltage V_g . The matrix elements $t_{jj'}$ represent hopping amplitudes between dot levels and $U_{jj'}^{\sigma\sigma'}$ describes electron-electron interactions. Of course, $U_{jj}^{\sigma\sigma} = 0$.

The non-interacting lead electrons created (annihilated) by $c_{j\sigma l}^\dagger$ ($c_{j\sigma l}$) at the Fermi surface of the right lead ($l = R$) and left lead ($l = L$) are described by the

Hamiltonian

$$H_E = -\tau_h \sum_{j\sigma l} c_{j\sigma l}^\dagger c_{(j+1)\sigma l} + h.c. \quad (27)$$

with a hopping amplitude τ_h between neighboring sites. The coupling of the leads to the quantum dot levels is modeled by a tunneling Hamiltonian

$$H_{DE} = - \sum_{j\sigma l} t_j^l c_{0,\sigma,l}^\dagger d_{j,\sigma} + h.c. \quad (28)$$

where electrons can tunnel from or to the dot levels from site 0 of the right or left lead. The tunneling matrix elements t_j^l are assumed to be real in the present paper. They determine the broadening of the dot levels as will be discussed in more detail below.

The Hamiltonian H is translated into an action suitable for a coherent state path integral formulation (see e.g., Ref. 13) essentially by replacing creation and annihilation operators by corresponding Grassmann variables. Physical observables at temperature $T = 0$ are obtained from the renormalized Green’s functions of the correlated dot system (see Eq. (17)),

$$g_{ij}^{-1}(i\omega) = i\omega\delta_{ij} + a_{ij,k=0}. \quad (29)$$

In a static approximation, the $a_{ij,k=0}$ do not depend on ω . The dot Green’s functions g are $N \times N$ matrices where N is the total number of electronic states included in the description of the quantum dot system. The matrix elements of the dot Hamiltonian $\epsilon_{j\sigma} + V_g$, $t_{jj'}$, and $U_{jj'}^{\sigma\sigma'}$ provide the necessary initial values for the corresponding flow equations. All other flow equations start the flow from an initial value of zero.

Since the dot system is coupled to the leads via the tunneling Hamiltonian H_{DE} , the dot levels acquire an imaginary part which is determined using a standard projection of the full Hamiltonian on the dot Hamiltonian as described in detail e.g. in Refs. 14 and 15,

$$\tilde{g}_{ij}^{-1}(i\omega) = i\omega\delta_{ij} + a_{ij,k=0} - i\text{sgn}(\omega)\Delta_{ij} \quad (30)$$

with the imaginary part given by

$$\Delta_{ij} = \pi\rho_0 \sum_{l=L,R} t_i^l t_j^l \quad (31)$$

in terms of the density of states of the lead electrons at the Fermi level $\rho_0 \approx 1/(\pi\tau_h)$ (in the wide band approximation). Usually, the absolute values of the tunneling matrix elements are given in terms of the parameters $\Gamma_i^l = \pi\rho_0(t_i^l)^2$.

From this propagator, the average dot occupancies $\langle n_{j\sigma} \rangle$ at $T = 0$ may be easily calculated using

$$\langle n_{j\sigma} \rangle = \frac{1}{2\pi} \int_{-\infty}^{\infty} d\omega e^{i\omega 0^+} \tilde{g}(i\omega). \quad (32)$$

where the exponential factor enforces convergence of the integral at large ω . To relate the dot propagator to the

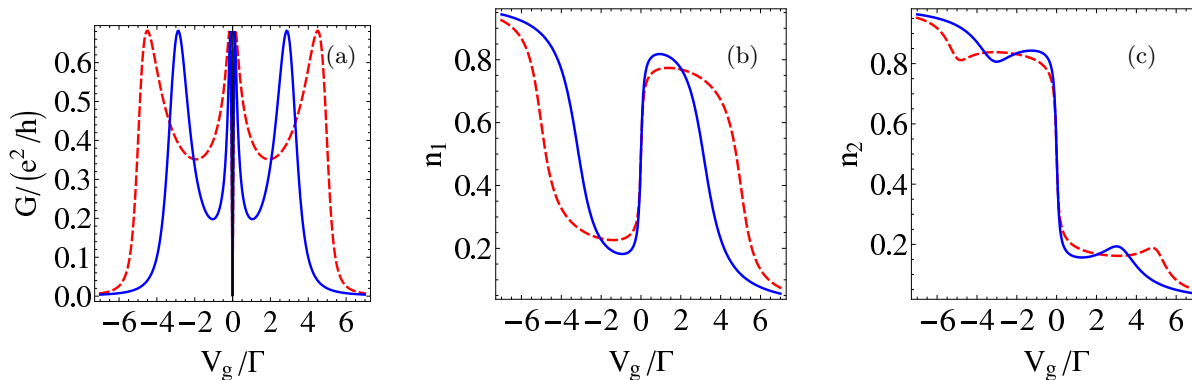


FIG. 2: (color online) Conductance \mathcal{G} (a) and occupancies n_1 (b) and n_2 (c) for a polarized double dot, $U/\Gamma = 8$, $\Gamma_1^L = 0.27\Gamma$, $\Gamma_1^R = 0.33\Gamma$, $\Gamma_2^L = 0.16\Gamma$, $\Gamma_2^R = 0.24\Gamma$, $t_2^R < 0$ all other t_i^L positive, dashed lines: truncation at $m = 1$, full lines: truncation at $m = 2$.

conductance is quite an intricate problem which has been addressed using both the Landauer-Büttiker¹⁶ and the Kubo formalism¹⁷. At $T = 0$, one obtains for the conductance \mathcal{G} the rather intuitive result

$$\mathcal{G} = 4 \frac{e^2}{h} \left| \sum_{i,j} \pi \rho_0 t_i^R t_j^L \tilde{g}_{ij}(0) \right|^2 \quad (33)$$

where the sum runs over all dot levels connected to the leads via non-vanishing tunneling matrix elements t_j^L . The phase of the sum in Eq. (33) is known as the transmission phase. This quantity is accessible experimentally and will be also briefly discussed in the following.

A. Polarized double dot

We first review calculations for a polarized double dot corresponding to two states with $\epsilon_{1\sigma} = \epsilon_{2\sigma} = 0$. Each state is occupied by only one electron as depicted in Fig. 1. The system is spin polarized, which may be achieved by putting it into a strong magnetic field. Studies of this system using different methods were presented e.g., by König and Gefen¹, Sindel *et al.*² as well as Meden and Marquard³.

The effective potential for this problem corresponds to Eq. (3) and the flow equations for the running couplings are given by Eq. (21). It is very easy to solve these equations numerically. In Fig. 2 we show results for the parameter set given in the figure caption. This parameter set with the rather large Coulomb interaction $U/\Gamma = 8$ and $t_{12} = 0$ has been taken from Ref. 3. (For convenience, here and in the following all energies will be given in units of $\Gamma = \sum_{il} \Gamma_i^l$.) The figure shows Coulomb correlation induced resonances close to $V_g = 0$. The dashed curves agree with the results of Ref. 3, which were calculated neglecting the renormalization of the Coulomb interactions. The full curves include this renormalization, and

the figure clearly shows its importance (see also Ref. 18). We would like to emphasize, that within the static approximation, there are no higher order vertex functions to be considered, since the set of equations (21) is complete. It is therefore possible to apply these equations at even larger Coulomb interactions. One finds that with increasing Coulomb interactions the two outer Coulomb blockade peaks seen in Fig. 2 shift further outwards and the exponentially sharp correlation induced peaks in the center shift exponentially close to zero. The dot level occupancies displayed in Fig. 2 show the characteristic charge oscillations discussed in detail in Refs. 1 and 2.

B. Side coupled double dot

Now we consider a side coupled double dot with spin as depicted in Fig. 4. Only one dot is coupled to the leads directly. For this system, the set of coupled flow equations is much more complicated than for the polarized double dot briefly reviewed above, and higher order equations $m > 2$ play a role. In fact, assuming spin symmetric interactions, we have to solve a set of 26 coupled equations as was pointed out before. We will investigate two physically different cases: large interdot hopping $t_{12} > \Gamma$ and small interdot hopping $t_{12} < \Gamma$. In both cases we study the influence of intra-dot Coulomb interactions U , which are chosen to be equal on both quantum dots. Inter-dot Coulomb interactions are set initially to zero, but they evolve to finite values during the renormalization run. In fact, all 26 running couplings (vertex functions) considered here renormalize to non-zero values in certain gate voltage ranges, some of them attaining extremely large values. Side coupled double dots have been investigated by Cornalia and Grepel¹⁹ and Zitko and Bonca²⁰ using the NRG as well as Karrasch, Enss and Meden⁴ using the fRG truncated at $m = 2$.

We start with a discussion of dot systems with large interdot hopping described by the parameter set $t_{12}/\Gamma = 4$,

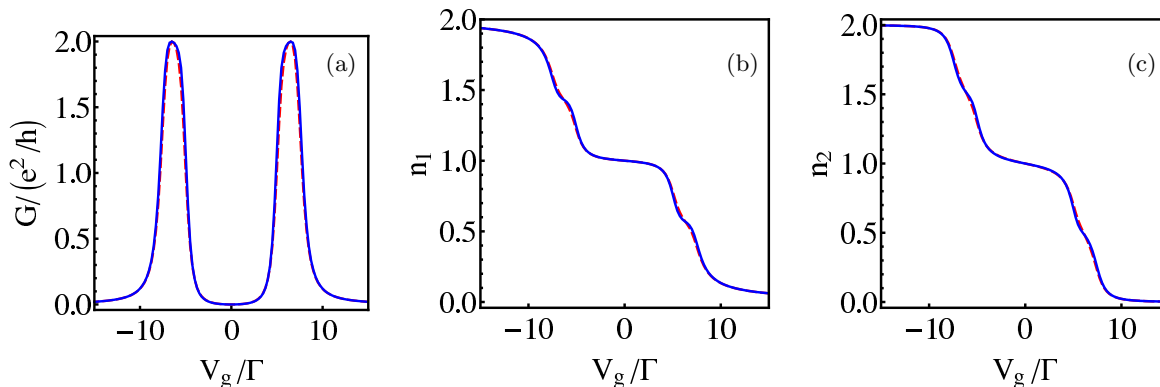


FIG. 3: (color online) Side coupled double dot with large interdot hopping: $t_{12}/\Gamma = 4$, $U/\Gamma = 8$, $\Gamma_1^L = \Gamma_1^R = \Gamma/2$, full lines: truncation order $m = 4$, dashed lines: truncation order $m = 2$, (a) conductance \mathcal{G} , (b) occupancy of directly coupled dot n_1 , (c) occupancy of side coupled dot n_2 .

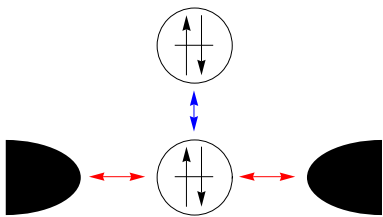


FIG. 4: (color online) Side-coupled quantum dot device.

$U/\Gamma = 8$, and $\epsilon_{1\sigma} = \epsilon_{2\sigma} = 0$ and other parameters given in the caption of Fig. 3. The same parameter set was discussed in Refs. 4 and 19. Rough estimates discussed in Ref. 19 suggest that one should observe conductance peaks located at $V_g \approx \pm(U/2 + t_{12})$ with a width given by $U/2$. This is indeed seen in Fig. 3(a). In this figure, we compare calculations truncated at different flow orders. The dashed curves show calculations truncated at $m = 2$ as in Ref. 4. The full curves include all orders up to $m = 4$, which is the maximum order possible in this system. We observe that the inclusion of the higher orders has the effect of somewhat increasing the width of the peaks in accordance with the NRG calculations presented in Ref. 19. The dot occupation numbers [Fig. 3(b) and (c)] show slightly more pronounced shoulders if higher order effects $m > 2$ are included within the gate voltage ranges of peak conductance.

Now we increase the intra-dot Coulomb interaction to $U/\Gamma = 12$. According to the discussion presented in Ref. 20, the peaks should become a more box-like in shape. This is indeed seen in Fig. 5(a), but only if the higher order contributions $m > 2$ are included. A calculation truncating the set of equations at $m = 2$ shows conductance peaks with a Lorentzian shape in disagreement with NRG calculations²⁰. The conductance peaks shown in Fig. 5(a) are not completely flat as suggested by the NRG calculations. This probably points to effects beyond the static approximation employed here. The occupancies of the two dots are shown in Fig. 5(b) and (c).

Here the effect of higher order contributions is quite important as well. The single occupancies n_i even show a non-monotonic behavior in the gate voltage ranges of peak conductance. Similarly, the transmission phase develops a shoulder in these gate voltage ranges which is not seen in calculations truncated at $m = 2$.

If one increases the intra-dot Coulomb interaction further, e.g., to $U/\Gamma = 16$, one observes conductance peaks which are flat, but within this flat region the renormalization procedure employed here becomes ill defined. Technically, this can be traced to the fact that somewhere along the renormalization flow the renormalized self energies of the indirectly coupled dot vanish. At this point the body of the matrix K which was introduced in the previous section vanishes, all flow equations develop a singularity, and the renormalization flow stops. The singular renormalization flow likely indicates a failure of the static approximation.

Let us now discuss a physical situation with small inter-dot hopping: Fig. 6 shows a calculation using the parameters $t_{12}/\Gamma = .2$ and $U/\Gamma = 2$, $\epsilon_{1\sigma} = \epsilon_{2\sigma} = 0$. This parameter set was also investigated in Refs. 4 and 19. As was pointed out by the authors of Ref. 4, the calculation truncated at $m = 2$ yields a conductance minimum, which is too flat in comparison to NRG calculations¹⁹. As is obvious from Fig. 6(a) inclusion of higher order effects improves this situation. However, comparison with the NRG data presented in Ref. 19 still shows quantitative differences in this gate voltage region. Since our calculations are not truncated within the constraints of the static approximation, these differences must be attributed to effects beyond the static approximation.

Of course, the structure obtained for the conductance and the occupancies as a function of the gate voltage can be related to the calculated spectrum of the dot system. In Fig. 7 we show the energy level for a spin up electron on the directly coupled dot given by a_{11} and the energy level of a spin up electron on the side-coupled dot a_{33} for the parameter set used in Fig. 6. Again we compare calculations truncated at $m = 2$ with a full calculation

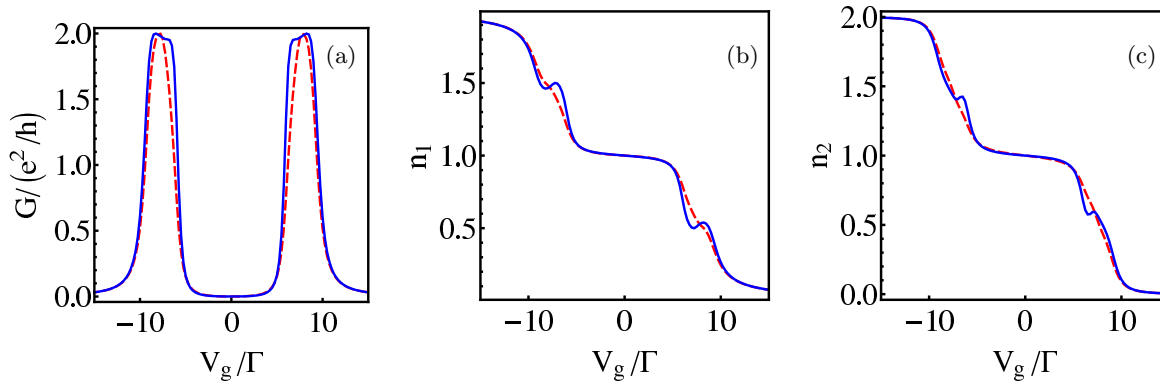


FIG. 5: (color online) Side coupled double dot with large interdot hopping: $t_{12}/\Gamma = 4$, $U/\Gamma = 12$. Other parameters and notation as in Fig. 3

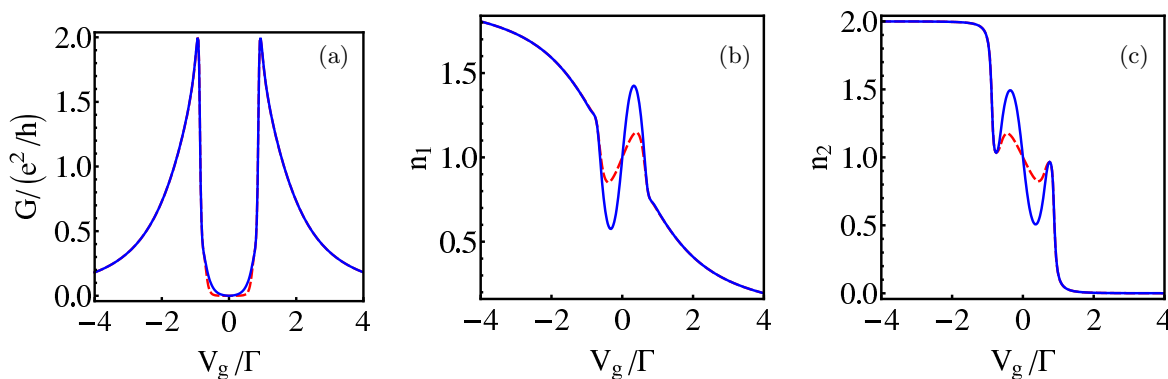


FIG. 6: (color online) Side coupled double dot with small interdot hopping $t_{12}/\Gamma = .2$, $U/\Gamma = 2$. Other parameters and notation as in Fig. 3

in the static approximation. Obviously, truncating at $m = 2$ yields significantly too small energy eigenvalues in particular for the indirectly coupled dot.

If we increase the intra-dot Coulomb interaction from $U/\Gamma = 2$ to $U/\Gamma = 2.5$, we observe a picture similar to the one shown in Fig. 6 with the amplitude of the charge oscillations on the dots significantly increased. Already for $U/\Gamma = 3$, the set of flow equations develops singular behavior as was discussed above for the case with large inter-dot hopping. This again indicates that a truncation scheme based on a static approximation fails for large Coulomb interactions.

C. Parallel coupled double dot

Finally we consider a parallel coupled double dot as depicted in Fig. 8. The set of equations to be solved is the same as for the side-coupled dot.

We study a parameter set where all t_i^l are chosen positive with the tunneling strengths Γ_i^l given numerically in the caption of Fig. 9. We choose $U_{jj'}^{\sigma\sigma'}/\Gamma = 2$ for all intra-dot and inter-dot interaction matrix elements and

$t_{12} = 0$. This parameter set has also been investigated in Ref. 4. Due to the large Coulomb interaction, correlation induced resonances are observed similar to the spin-polarized system briefly reviewed in section III A. However, as is seen in Fig. 9 calculations truncated at $m = 2$ show significant quantitative differences in comparison to the full calculation up to $m = 4$: The resonances are much more pronounced and the valley between these resonances is somewhat narrower. This trend continues, if we increase the Coulomb interactions to $U_{jj'}^{\sigma\sigma'}/\Gamma = 4$. Results are shown in Fig. 10. The amplitude of the charge oscillations of the dot with the stronger tunnel coupling to the leads is significantly underestimated in a calculation neglecting higher order contributions.

Of course, the question arises, to what extent the static approximation is still valid in this parameter region. In order to answer this question calculations beyond the static approximation must be performed. Such calculations are presently under way.

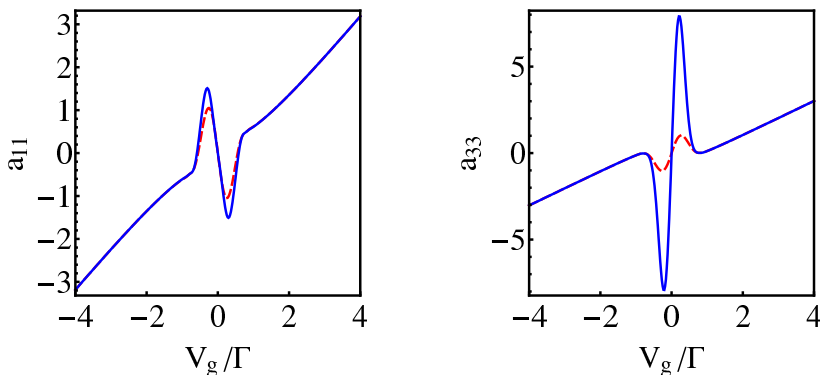


FIG. 7: (color online) Energy eigenvalues of the spin up level in directly coupled dot (a_{11}) and the indirectly coupled dot (a_{33}) as a function of the gate voltage for the parameter set of Fig. 6.

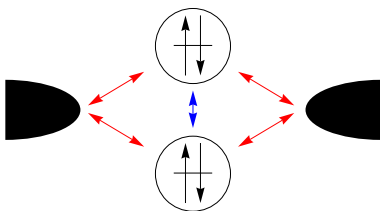


FIG. 8: (color online) Parallel coupled quantum dot.

IV. CONCLUSIONS

The functional renormalization group has been proposed as a useful new tool for the investigation of interacting mesoscopic systems^{3,4}. The advantage of the method in comparison to NRG or DMRG calculations appears to be its rather moderate numerical cost. However, this advantage is due to some rather drastic approximations, which are not easily controlled. In this paper we carry out the first steps that are needed to go beyond the standard set of approximations usually employed to solve the fermionic fRG in practice. Still within the constraints of a static approximation we develop a method which systematically generates the complete set of ordinary differential equations corresponding to the fRG. However, the method proposed here is not limited to the static approximation. It can be extended straightforwardly to include non-static effects e.g. by including a wave function renormalization in the kinetic energy term of the action.

We demonstrate by means of a number of calculations of transport properties of quantum dot systems that

inclusion of higher order equations definitely improves fRG calculations for large Coulomb interactions. This is judged by a comparison to NRG results. However, if one increases Coulomb interactions beyond some critical value, the static approximation fails as is signalled by singularities developing during the renormalization flow. In order to overcome such problems and to further improve the agreement between NRG and fRG calculations it is necessary to go beyond the static approximation. Work in this direction is presently under way.

Acknowledgments

M.W. would like to thank Volker Meden for many useful discussions and Christoph Karrasch for providing detailed results of his calculations. We thank Marcel Regnatto for suggestions in the early stages of this work and a careful reading of the manuscript.

APPENDIX A: INTEGRAL OVER THE MATSUBARA FREQUENCIES

In order to perform the rather singular integral over the Matsubara frequencies ω for the hard cutoff regulator Eq. (14) we need the formula²¹

$$\delta(x-y)f(\theta(x-y)) \rightarrow \delta(x-y) \int_0^1 ds f(s). \quad (\text{A1})$$

The ω -integration leading from Eq. (11) to Eq. (15) is then performed as follows

$$\begin{aligned} & \text{Tr} \int_{-\infty}^{\infty} \frac{d\omega}{2\pi} (G^{-1}(i\omega) + Ck\theta(k^2 - \omega^2)\mathbb{E})^{-1} \frac{\partial}{\partial k} Ck\theta(k^2 - \omega^2) \\ &= \frac{2N}{\pi} + \text{Tr} \int_{-\infty}^{\infty} \frac{d\omega}{2\pi} (G^{-1}(i\omega) + Ck\theta(k^2 - \omega^2)\mathbb{E})^{-1} 2Ck^2\delta(k^2 - \omega^2) \end{aligned} \quad (\text{A2})$$

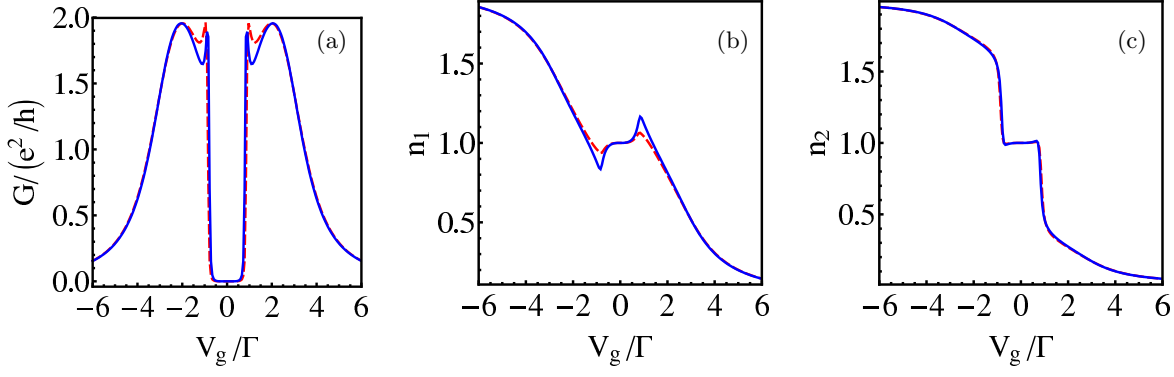


FIG. 9: (color online) Parallel coupled double dot $t_{12}/\Gamma = 0$, $U/\Gamma = 2$, $\Gamma_1^L/\Gamma = .5$, $\Gamma_1^R/\Gamma = .25$, $\Gamma_2^L = 0.07$, $\Gamma_2^R = 0.18$. Other notation as in Fig. 3

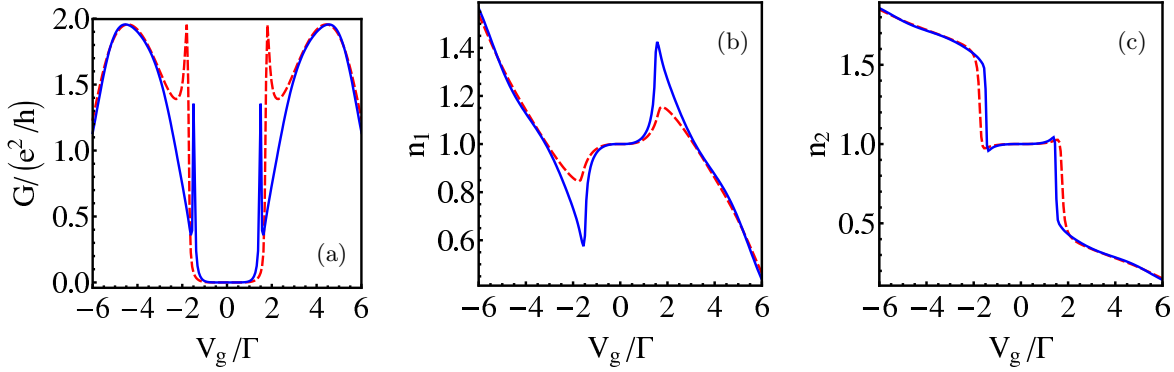


FIG. 10: (color online) Parallel coupled double dot $t_{12}/\Gamma = 0$, $U/\Gamma = 4$, $\Gamma_1^L/\Gamma = .5$, $\Gamma_1^R/\Gamma = .25$, $\Gamma_2^L = 0.07$, $\Gamma_2^R = 0.18$. Other notation as in Fig. 3

with $G^{-1}(i\omega) = (i\omega + u_k^{(2)})\mathbb{E}'$. The quantity $u_k^{(2)}$ represents the body of $U_k^{(2)}$. In the first term we already performed the limit $C \rightarrow \infty$. The second term is now evaluated with the help of Eq. (A1)

$$\begin{aligned} & \text{Tr} \int_{-\infty}^{\infty} \frac{d\omega}{2\pi} \left((G^{-1}(i\omega) + Ck\theta(k^2 - \omega^2)\mathbb{E})^{-1} \right. \\ & \quad \left. Ck(\delta(k - \omega)) + \delta(k + \omega) \right) \\ &= \frac{1}{2\pi} \sum_{\lambda=\pm k} \text{Tr} \int_0^C ds' \left(\frac{1}{k} G^{-1}(i\lambda) + s' \mathbb{E} \right)^{-1} \\ &= -\frac{1}{2\pi} \sum_{\lambda=\pm k} \text{Tr} \log \left(\frac{1}{k} G^{-1}(i\lambda) \right) + O(\log C) \end{aligned}$$

Therefore we obtain the equation

$$a'_0 = \frac{1}{4\pi} \sum_{\lambda=\pm k} \log \det \left(\frac{1}{k} G^{-1}(i\lambda) \right)$$

The infinite constant gets absorbed into a suitably modified initial condition.

With similar steps as above one obtains the result given in Eq. (16). Here it is important to use the fact that the factors under the trace may be permuted cyclically.

* Electronic address: michael.weyrauch@ptb.de

¹ J. König and Y. Gefen, Phys. Rev. B **71**, 201308(R) (2005).

² M. Sindel, A. Silva, Y. Oreg, and J. von Delft, Phys. Rev. B **72**, 125316 (2005).

³ V. Meden and F. Marquardt, Phys. Rev. Lett. **96**, 146801

(2006).

⁴ C. Karrasch, T. Enss, and V. Meden, Phys. Rev. B **73**, 235337 (2006).

⁵ V. Kashcheyevs, A. Schiller, A. Aharony, and O. Entin-Wohlman, Phys. Rev. B **75**, 115313 (2007).

- ⁶ L. L. Sohn, L. P. Kouwenhoven, and G. Schön, *Mesoscopic Electron Transport* (Kluwer, Dordrecht, 1997).
- ⁷ J. Berges, N. Tetradis, and C. Wetterich, *Phys. Rep.* **363**, 223 (2002).
- ⁸ R. Hedden, V. Meden, T. Pruschke, and K. Schönhammer, *J. Phys.: Condens. Matter* **16**, 5279 (2004).
- ⁹ M. Weyrauch, *J. Phys. A* **39**, 649 (2006).
- ¹⁰ M. Salmhofer, *Renormalization. An Introduction* (Springer, 1999).
- ¹¹ C. Wetterich, *Phys. Lett. B* **301**, 90 (1993).
- ¹² V. Meden and U. Schollwöck, *Phys. Rev. B* **67**, 035106 (2003).
- ¹³ J. W. Negele and H. Orland, *Quantum Many-Particle Systems* (Perseus Books, Reading, MA, 1998).
- ¹⁴ A. Hewson, *The Kondo problem to heavy Fermions* (Cambridge University Press, ISBN 0-512-59947-4, 1993).
- ¹⁵ T. Enss, V. Meden, S. Andergassen, X. Barnabé-Thériault, W. Metzner, and K. Schönhammer, *Phys. Rev. B* **71**, 155401 (2005).
- ¹⁶ H. Bruus and K. Flensberg, *Many-Body Quantum Theory in Condensed Matter Physics* (Oxford University Press, 2004).
- ¹⁷ T. Enss, Ph.D. thesis, Max-Planck-Institut für Festkörperforschung, Stuttgart (2005).
- ¹⁸ C. Karrasch, T. Hecht, A. Weichselbaum, J. von Delft, Y. Oreg, and V. Meden, *New J. Phys.* **9**, 123 (2007).
- ¹⁹ P. S. Cornaglia and D. R. Grempel, *Phys. Rev. B* **71**, 075305 (2005).
- ²⁰ R. Zitko and J. Bonca, *Phys. Rev. B* **73**, 035332 (2006).
- ²¹ T. R. Morris, *Int. J. Mod. Phys. A* **9**, 2411 (1994).